Marine Geology 404 (2018) 1–14

Contents lists available at ScienceDirect

Marine Geology

journal homepage: www.elsevier.com/locate/margo

Storm impacts on hydrodynamics and suspended-sediment fluxes in a microtidal back-barrier estuary

D.J. Nowacki*, N.K. Ganju

U.S. Geological Survey, Woods Hole, MA, USA

A B S T R A C T

Recent major storms have piqued interest in understanding the responses of estuarine hydrodynamics and sediment transport to these events. To that end, flow velocity, wave characteristics, and suspended-sediment concentration (SSC) were measured for 11 months at eight locations in Chincoteague Bay, MD/VA, USA, a shallow back-barrier estuary. Daily breezes and episodic storms generated sediment-resuspending waves and modified the flow velocity at all sites, which occupied channel, shoal, and sheltered-bay environments with different bed-sediment characteristics. Despite comparable SSC during calm periods, SSC at the channel locations was considerably greater than at the shoal sites during windy periods because of relatively more erodible bed sediment in the channels. Sediment fluxes were strongly wind modulated: within the bay's main channel, depth-integrated unit-width sediment flux increased nonlinearly with increasing wind speed. When averaged over all sites, about 35% of the flux occurred during windy periods (wind speed greater than 6 m s^{-1}), which represented just 15% of the deployment time. At channel sites, the net water and sediment fluxes were opposite to the direction of the wind forcing, while at shoal sites, the fluxes generally were aligned with the wind, implying complex channel–shoal dynamics. Yearly sediment fluxes exceed previous estimates of sediment delivery to the entirety of Chincoteague Bay. These observations illustrate the dynamic sedimentary processes occurring within microtidal back-barrier lagoons and highlight the importance of storm events in the hydrodynamics and overall sediment budgets of these systems.

1. Introduction

Barrier islands make up about 10% of all continental shorelines, and occupy nearly 2300 km of the Atlantic coast of North America (Stutz and Pilkey, 2011). The lagoons that form landward of these barriers, extensive along the U.S. Atlantic and Gulf coasts, are important and dynamic sedimentary environments forming a key role in landward island transgression. Despite considerable attention paid to the sand dynamics of barrier islands, the sediment-transport regime of tidal inlets, and lagoon sedimentation, comparatively little research has been conducted on fine-sediment dynamics within back-barrier lagoons. Understanding these dynamics is crucial because every element of a barrier-island system influences or is influenced by the lagoon (Oertel, 1985).

Among other roles, back-barrier estuaries provide critical habitat for seagrass and salt marsh, and grounds for commercially important fisheries. These habitats are preferentially located in particular geomorphic settings, which can themselves modify the bathymetry and resultant water circulation (Ralston et al., 2010; Ralston et al., 2012; Defne and Ganju, 2015), sediment transport (Dronkers, 1986), and depositional regimes of the estuary (Nichols and Allen, 1981). Morphology of back-barrier estuaries also is closely linked to wave action, ecosystem functions, and water quality.

Because back-barrier estuaries tend to be low-pass filters, damping tides but allowing propagation of subtidal (i.e., longer than a tidal cycle) motions (Wong and Wilson, 1984; Aretxabaleta et al., 2014), forcing at periods other than tides becomes important in these environments. For example, wind forcing, in both its local and remote forms, is a major controlling influence on circulation (Chant, 2001), sediment resuspension (Wells and Kim, 1989; Nichols and Boon, 1994), and larval supply variability (Xie and Eggleston, 1999). Storms may also temporarily change lagoons from sediment sinks to sediment sources, and vice versa (Nichols and Boon, 1994).

Coastal lagoons tend to trap inorganic sediment and organic matter (Kjerfve, 1994) but are not necessarily passive features destined to infill with sediment (Nichols and Boon, 1994). Sediment delivered to back-barrier estuaries is generally a combination of riverine input, shoreline erosion, overwash or aeolian transport from barrier islands, and delivery from the coastal ocean (Nichols and Allen, 1981); reworking of sediment on the lagoon seabed can also be considerable (Nichols and Boon, 1994). Understanding how sediment fluxes can both modify and be controlled by local and regional morphology can lead to greater insight to how these systems evolve and how they may change in the face of changing sediment supply, connectivity with the ocean, and rising sea level. Sediment fluxes during fairweather and storm conditions are critical in determining the resilience of marsh systems that

* Corresponding author.
E-mail address: dnowacki@usgs.gov (D.J. Nowacki).

https://doi.org/10.1016/j.margeo.2018.06.016
Received 31 July 2017; Received in revised form 23 April 2018; Accepted 27 June 2018
Available online 01 July 2018

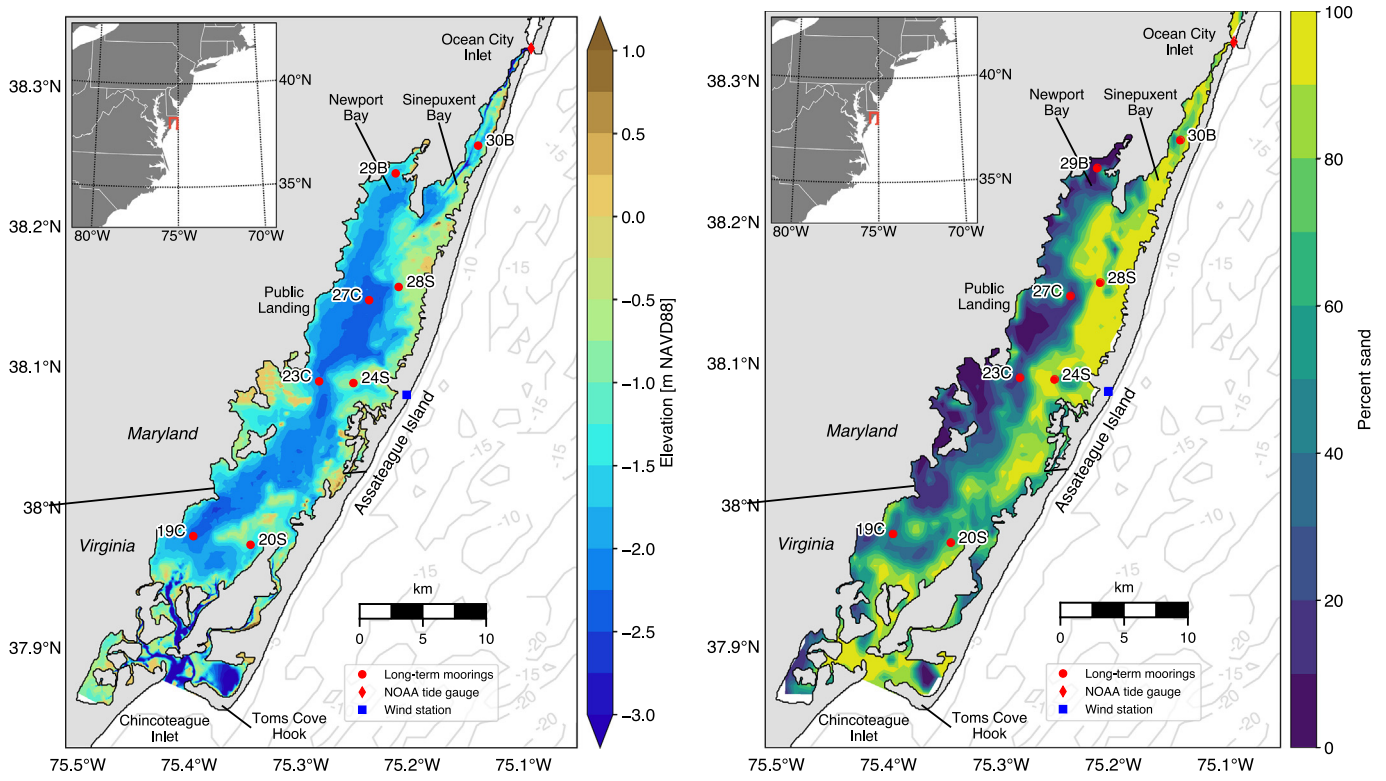

Fig. 1. (Left) Bathymetric map of Chincoteague Bay showing locations of moorings, the NOAA tide gauge at Ocean City, MD, and the wind station on Assateague Island. (Right) Map showing bed-sediment sand fraction in Chincoteague Bay (National Park Service, 2017). Darker colors indicate regions of finer sediment. (For interpretation of the references to color in this figure legend, the reader is referred to the web version of this article.)

protect habitat, shorelines, and communities, and a better understanding helps inform restoration and preservation of these systems.

In this work, we present results from an 11 month study of hydrodynamics and sediment transport within Chincoteague Bay, MD/VA, a back-barrier estuary on the mid-Atlantic coast of the United States. We describe the characteristics of fine-sediment transport under both calm and stormy conditions and emphasize the importance of storms in this microtidal environment. We decompose the processes driving the sediment flux and characterize the long-term sediment fluxes at diverse locations within the bay. The observed subtidal velocity patterns are shown to be reproducible with a relatively simple analytical model and describable with empirical orthogonal functions. We compare our observed fluxes to previous estimates of sediment delivery to the bay and consider the importance of morphology in this system.

1.1. Study site

Chincoteague Bay is a coastal-plain back-barrier lagoon separated from the Atlantic Ocean by Assateague Island, the northernmost undeveloped barrier island on the U.S. East coast (Fig. 1). The bay is about 55 km in length and 10 km in width, has a surface area of 417 km^2, and is oriented NNE–SSW. Ocean City Inlet and Chincoteague Inlet are the only present connections to the Atlantic Ocean. There are two subembayments at the north end of the bay. Newport Bay is a small, sheltered bay at the extreme northwest of Chincoteague Bay. It is a flooded extension of Trappe Creek and receives about one quarter of the freshwater that enters Chincoteague Bay despite occupying only about four percent of the surface area. The estimated mean freshwater input to Newport Bay is 1.5 $m^3 s^{-1}$. Sinepuxent Bay, immediately to the east of Newport Bay, is a long, narrow basin that connects Chincoteague Bay and Ocean City Inlet.

Chincoteague Bay has an average depth of 1.4 m, and is characterized by a deep (~3 m) basin (the "channel") in the central-to-western section of the bay, which shallows toward the eastern side (the "shoal"). Chincoteague Bay is microtidal, with tidal ranges greatest near the inlets (~1 m) that rapidly diminish from friction, resulting in a mean tidal range of 0.16 m at Public Landing.

As described by Bartberger (1976), approximately equal quantities of sand and mud are supplied to Chincoteague Bay from two principal sources. The sand comes primarily from Assateague Island, both from storm overwash and from aeolian transport, and this material makes up much of the shoal areas (Fig. 1). Mud comes from the mainland, mostly from marsh erosion; winds have been shown to undercut tidal-marsh root mat and lead to marsh erosion in Chincoteague Bay (Krantz et al., 2009) and wind-wave power is linearly correlated with marsh erosion (Leonardi et al., 2016). Local streams provide a small (< 10%) additional fine-sediment source. This finer material is prevalent throughout the channel (Fig. 1). The total annual sediment delivery to Chincoteague Bay is about 0.1 Mt y^{-1}, although more recent studies using radiochemical methods suggest an annual sediment delivery of 1 Mt y^{-1} or more (Wells et al., 1997, 1998, Wegner et al., 2011).

Chincoteague Bay experiences two main categories of storms: cold-core extra-tropical storms (nor'easters) during the fall and winter, and hurricanes during summer and fall. Fall and winter storms generally feature winds with a northern component, while summer winds are mostly from the SSW (Carruthers et al., 2011). These storm wind patterns are approximately aligned with the longitudinal axis of the bay; winds are particularly important in Chincoteague Bay because they have a greater effect on water levels and currents than do tides (Casey and Wesche, 1981).

The importance of wind in Chincoteague Bay has also been confirmed via numerical modeling: wind dominates water and salt flux at higher wind speeds, while tides are most important at lower wind speeds (Kang et al., 2017). These findings are consistent with previous studies which have emphasized the importance of wind on estuarine hydrodynamics, salinity structure, and sediment transport (Goodrich,

1988; Wells and Kim, 1989).

2. Methods

2.1. Field deployments

Eight bottom-mounted oceanographic platforms (Fig. 1) were deployed from 13 August 2014 to 12 July 2015, to measure flow velocity, suspended-sediment concentration (SSC), waves, and other water-quality parameters. Six platforms (19C & 20S, 23C & 24S, 27C & 28S) were arranged in channel–shoal pairs to assess the differences in hydrodynamics and sediment dynamics of these contrasting geomorphic settings, which are distinct in depth and bed grain size (Fig. 1). Additionally, two platforms (29B, 30B) were deployed in Newport Bay and Sinepuxent Bay. The letter designators indicate the geomorphic setting: 'C' for channel, 'S' for shoal, and 'B' for Newport and Sinepuxent Bay.

Each platform was outfitted with either a 1 MHz or 2 MHz Nortek Aquadopp acoustic Doppler current profiler measuring currents throughout the water column. Turbidity and other water-quality parameters were measured with a YSI 6600 or YSI EXO2 multi-parameter sonde, or with a WET Labs ECO NTU turbidity sensor. Turbidity was converted to SSC using water samples collected in the field as described in the Supplementary Material. Waves were measured at all locations except 30B with an RBR, Ltd. RBRvirtuoso wave/tide gauge recording at 6 Hz, or with the wave-burst mode of the Aquadopp, recording at 2 Hz. Instruments were mounted nominally 0.15 m above the bed, and parameters were measured every 15 min(30 min for waves). After accounting for instrument servicing, fouling, and failure, the period of valid data at each of the eight moorings ranged between 92 and 319 days.

In order to provide meteorological context, wind data were obtained from Remote Automatic Weather Station ASTM2 on Assateague Island (Fig. 1).

2.2. Data processing

Data were processed as described in Suttles et al. (2017).

Wave statistics were computed with DIWASP version 1.4 (Johnson, 2011). Combined wave–current shear velocity u_{*wc} was computed following Madsen (1994). The Nikuradse roughness length was determined as $k_s = 2.5D_{50}$ (Soulsby, 1997), where D_{50} was the mean grain size of the bed-sediment sample closest to each station, using data from Ellis et al. (2015). Because waves were not measured at 30B, the computed shear velocity there is due only to currents.

The 15 minute data were low-pass filtered with a zero-phase, fifth-order Butterworth filter with a cutoff period of 35 h to remove tidal fluctuations but preserve subtidal signals.

2.2.1. Water and sediment fluxes

Unit-width water fluxes were computed as the product of the depth-averaged flow velocity and the water depth, multiplied by the 15 minute sampling interval. Suspended-sediment fluxes are the product of water fluxes and the near-bottom SSC under the assumption that sediment in suspension was well mixed. An analysis of uncertainty in the flux calculation is presented in the Supplementary Material.

2.2.2. Flux decomposition

To interpret the sediment fluxes, we implemented a flux decomposition procedure (e.g., Dyer, 1974). Although there are many possible approaches to flux decomposition, we computed it as:

$$F = \langle uhc \rangle = \underbrace{\langle\langle u\rangle\langle h\rangle\langle c\rangle\rangle}_{F_{adv}} + \underbrace{\langle u'\langle h\rangle c'\rangle}_{F_{disp}} + \underbrace{\langle u'h'\langle c\rangle\rangle}_{F_{stokes}} + \text{ small terms} \quad (1)$$

where u is depth-averaged velocity, h is water depth, c is SSC, angle brackets indicate tidally averaged (i.e., low-passed) values, and primes indicate deviations from the tidal average. The first term on the right-hand side is the advective flux, which arises from the average (subtidal) terms, and is associated with long-period forcing. The second term is the dispersive flux, attributable to the tidal-scale correlation between velocity and SSC. The third term is the Stokes-drift flux, arising from the correlation between velocity and depth when tides are progressive. Compared to these terms, the remaining five terms were small and we neglect them.

3. Results

3.1. General characteristics

Mean measured tidal range was largest at the southern end of Chincoteague Bay (about 27 cm) and decreased with distance northward. Mid bay, the range reduced to approximately 17 cm, and further diminished to about 12 cm in Sinepuxent Bay. That the smallest tidal range was observed at the location closest to Ocean City Inlet is evidence of the intense frictional damping within Sinepuxent Bay. Subtidal water-level variations arising from atmospheric and regional sea-level forcing approached 1 m, suggesting the importance of non-tidal influence in this system.

Flood tides flowed to the north, except for at 30B, where flood-tidal currents flowed to the south — i.e., the bay drains and fills simultaneously via both inlets. The tidal character was progressive near the inlets; mid-bay, at 23C and 24S, the tides were of a mixed progressive and standing character. In the north-central bay, the tides were nearly fully standing. Maximum currents generally were 0.3 m s^{-1} or less (Fig. 2). Despite a shorter flood-tide duration at most sites, maximum ebb-tidal currents within the main bay were 6–76% faster than floods. In Sinepuxent Bay, peak floods were stronger than ebbs; taken together, these ratios describe a pattern of stronger peak southward currents than those toward the north, suggesting southward residual transport.

Waves were larger in the channel than the shoal (Fig. 2), and wave height generally increased with distance northward in the bay, although waves in sheltered Newport Bay were the smallest of all locations. Averaged over all deployments and platforms, the mean significant wave height was 0.14 m; the maximum significant wave height was 0.88 m, at 23C. Mean wave period at all sites ranged from 1.5 to 2.1 s, indicating a wave field composed of locally generated seas.

When considering the full deployment at all sites, the average SSC was 30 mg L^{-1}, and SSC was generally greater in the channel than on the shoal (Fig. 2). Within the main-bay channel, SSC increased with distance northward. The smallest SSC was observed in Newport and Sinepuxent Bays at the extreme northern end of the bay; maximum SSC was 768 mg L^{-1}, at 23C.

3.2. Meteorological forcing

Compared to calm conditions, windy periods exhibited water-level variability, current modification, and increases in wave height and SSC (Fig. 2). As winds blew over the bay, water levels were modified, with setup at the downwind end of the bay and set-down upwind. The magnitude of the tidal currents in both directions in the channel increased, while flows at the shoal were more directly influenced by the wind, moving in the direction of the wind stress. Significant wave heights increased with the onset of wind, particularly at channel sites. Finally, SSC increased dramatically, especially at the channel sites, with the onset of wind and resulting wave activity. The increase in current speed and SSC together drove an increase in sediment flux at all locations during the storm.

After the wind subsided, the setup and set-down reduced, and water levels reverted to their fair-weather conditions in less than a single tidal cycle. Similarly, the significant wave heights and SSC in the channel reduced to background conditions almost immediately after the cessation of wind input. These patterns together indicate that the bay

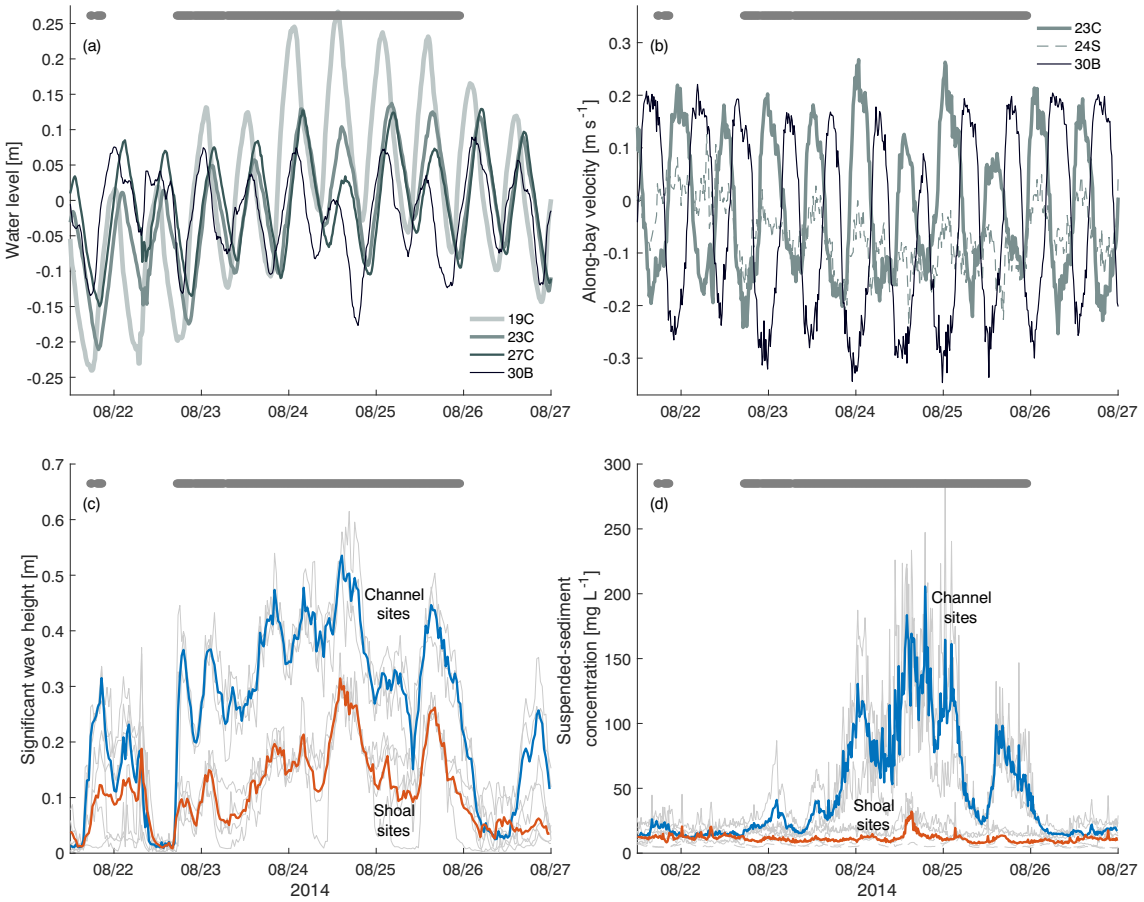

Fig. 2. (a): Water level at 19C, 23C, 27C and 30B. (b): Along-bay velocity at 23C, 24S, and 30B. (c): Significant wave height grouped by channel and shoal locations. (d) SSC grouped by channel and shoal locations during late August 2014. Grey markers at top of each panel indicate times when wind speed was greater than 5 m s^{-1} during a moderate ENE wind event. Note modification of water level and velocity and increase in waves and SSC during windy periods.

responds rapidly both to the onset and end of external wind forcing: sediment settles out of suspension, and water and sediment fluxes quickly return to their pre-wind values.

3.3. Processes driving sediment flux

The shallow depth of the bay enables rapid generation of waves with little lag between energy input from the wind and its corresponding wave-height response. Wind speed and wave height were highly correlated, and R^2 exceeded 0.9 at some sites (Fig. 3a). Correlation was greatest at the channel sites and least in Newport Bay (29B), likely because it is a sheltered, shallow subembayment with limited fetch in three directions. The maximum correlation between wind speed and waves occurred at zero lag, reinforcing the tight temporal relationship between wind and waves. The less-pronounced peaks in the cross-correlation at the shoal sites may be indicative of the depth-

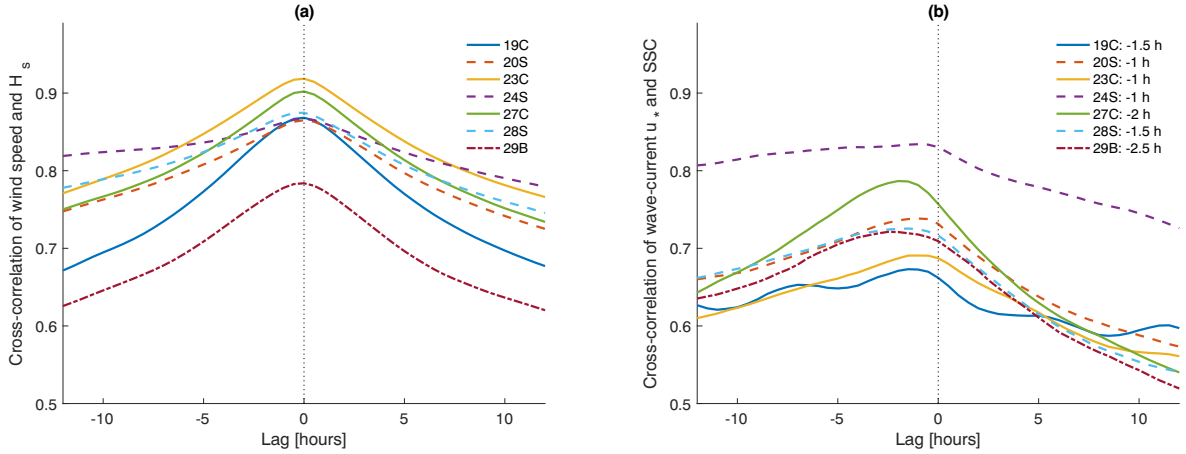

Fig. 3. (a): Cross-correlation of wind speed and significant wave height at seven moorings showing strong correlation between wind and waves and maximum correlation values at zero lag. (b): Cross-correlation of wave–current shear velocity and SSC at seven moorings. There is strong correlation between the shear velocity and SSC and a lag of 1–2.5 h at all moorings. The relatively short SSC record available at 24S is likely responsible for this site's anomalous trend in (b).

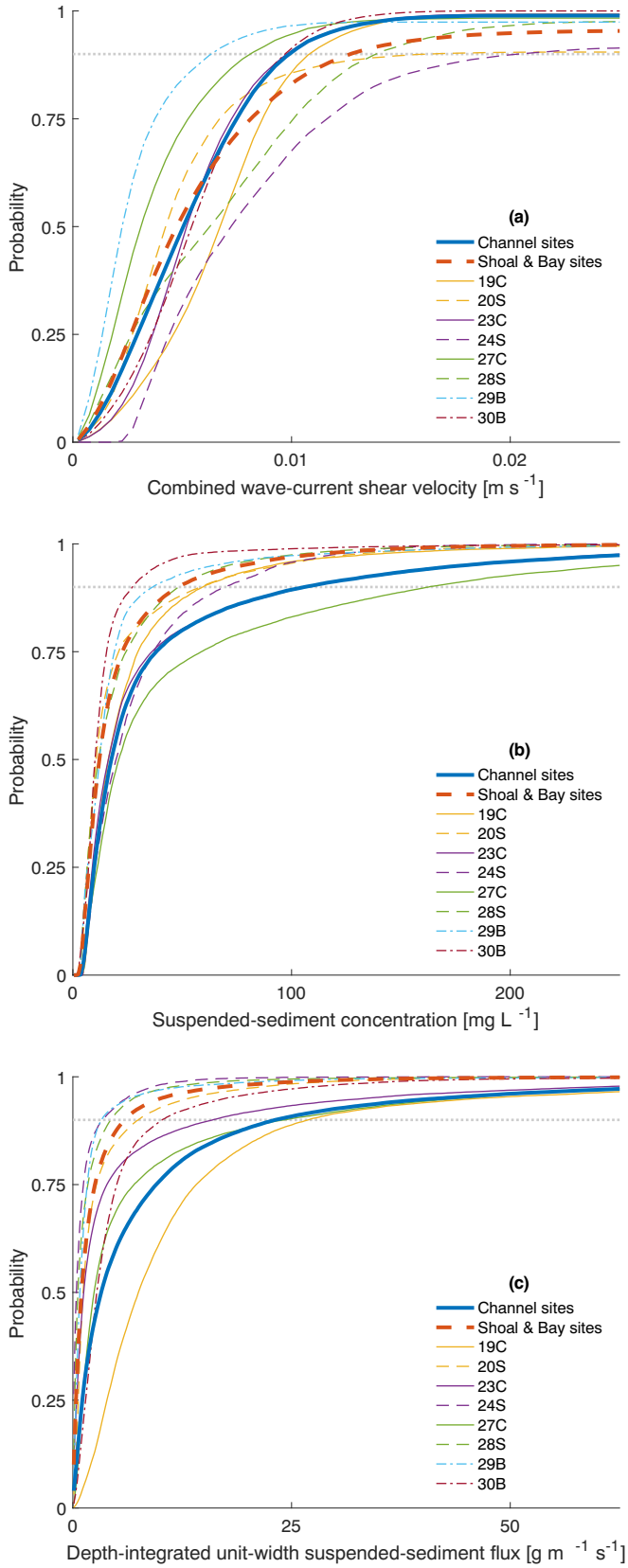

Fig. 4. Cumulative density plots of (a): combined wave-current shear velocity; (b): SSC; and (c): suspended-sediment flux at eight moorings. Heavy lines show distributions for all data of a given geomorphic setting; thin lines are distributions of individual sites. Because no wave data were available at 30B, the shear velocity for 30B shown in (a) are from currents only. Horizontal dotted line is at the 90th percentile.

limited nature of the waves there, where waves are unable to continue to grow with wind as they can within the channel.

As waves develop from wind input, wave-orbital motions apply stress to the seabed, and along with current-induced stress, can lead to local sediment resuspension. If the SSC at a given site were fully attributable to local resuspension, the cross-correlation between the bed stress and SSC would be 1. In Chincoteague Bay, u_{*wc} was well correlated with SSC, $0.65 < R^2 < 0.80$ (Fig. 3b). These values suggest the importance of local resuspension but also prevalence of sediment delivery by advection. In contrast to the zero lag between wind and waves, there is a lag of 1.0–2.5 h between the bed stress and SSC, suggesting either the presence of scour lag (van Straaten and Kuenen, 1958; Postma, 1967) or similar effects, or the delay of advective sediment delivery from elsewhere.

In order to synthesize parameters across the eight sites, we consider the probability distributions of u_{*wc}, SSC, and sediment flux at each location. The distribution of u_{*wc} helps determine the amount of bed stress and potential for local sediment resuspension at a given site. On average, values were comparable at both channel and shoal locations, although u_{*wc} in the channel was confined to a slightly narrower range (Fig. 4a). The 90th percentile shear velocities were nearly equivalent: 0.009 m s^{-1} at the channel sites and 0.011 m s^{-1} at the shoal sites. The distribution in Newport Bay was the lowest of all the sites, consistent with its weak waves and currents. Within these means, the largest u_{*wc} values were observed at 24S and 28S, which reflect the extensive fetch at these shoal locations. At the channel sites, the largest values were observed at 19C and 23C, which are exposed to maximum fetch during northeasterly storms.

Despite the slightly higher shear stresses observed at the shoal sites, the greatest SSC was in the channel (Fig. 4b), in particular at 23C and 27C; this pattern is also evident in Fig. 2. The greater SSC is likely a result of the more easily erodible, fine-grained sediment present at the channel sites (Fig. 1). Indeed, the 90th percentile SSC at the channel sites was 108 mg L^{-1}, while it was just 49 mg L^{-1} elsewhere. SSC was least in Newport Bay and Sinepuxent Bay, as was the case for u_{*wc}, because of the limited fetch at these locations.

The stronger velocities and greater SSC in the channels result in considerably greater suspended-sediment fluxes there, as compared to the shoals (Fig. 4c). The 90th percentile unit-width flux at the channel sites was 28.7 g m^{-1} s^{-1} and only 6.3 g m^{-1} s^{-1} at the other sites, indicating the overwhelming importance of the channel in transporting sediment on a unit-width basis.

Because of the tight correlation between wind, waves, bed stress, and SSC, particularly at channel sites, it is possible to develop relationships between an easily measurable quantity (wind speed) and more complex variables (SSC and suspended-sediment flux) (Fig. 5). These relationships have slopes which increase nonlinearly with wind speed. Data grouped by geomorphic setting collapse onto a clear trend line, and the means of aggregated data from each setting produce relationships of reasonable skill for moderate-to-strong winds (> 5 m s^{-1}). In the channel, SSC increases by 18 mg L^{-1} per 1 m s^{-1} increase in wind speed (range of all channel sites 12–23 mg L^{-1} per m s^{-1}); at the bay and shoal sites, slope is 6 mg L^{-1} per m s^{-1} (range 2–9 mg L^{-1} per m s^{-1}). Sediment flux values in the channel increase by 6.3 g m^{-1} s^{-1} per 1 m s^{-1} increase in wind (range 4.7–8.2 mg L^{-1} per m s^{-1}); at the bay and shoal sites, the slope is 1.2 g m^{-1} s^{-1} per m s^{-1} (range 0.7–1.8 g m^{-1} s^{-1} per m s^{-1}). When averaged over all sites, about 35% of the instantaneous sediment flux occurred when wind speed was greater than 6 m s^{-1}, which represented about 15% of the deployment time. The sharp increase in sediment flux at the channel sites is primarily a result of increased SSC during strong winds. The more moderate increase at the shoal sites is due to a combination of both increased flow velocity and SSC. The shallower slope at the shoal and bay sites is likely due to the minimal fetch at the bay sites and less-easily resuspendable sediment at the shoal sites. This pattern reflects the proximity of each setting to sediment sources, i.e., marsh at the

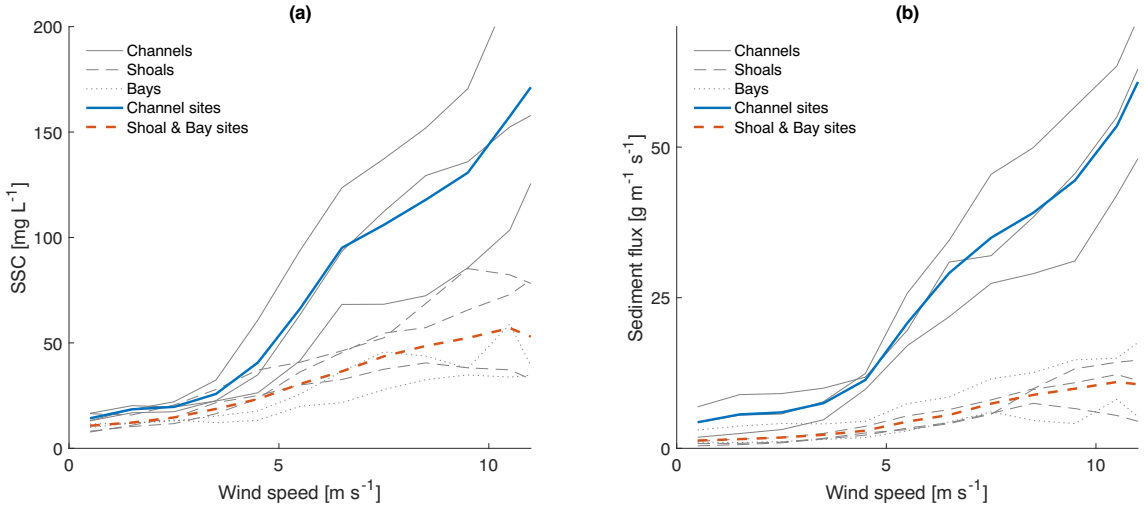

Fig. 5. Wind speed versus bin-averaged (a) SSC and (b) depth-integrated unit-width sediment flux at eight moorings. Note dramatic increases with wind speed at the channel sites. Traces represent averages in 1 m s^{-1} wind-speed bins.

channel sites and the barrier at the shoal sites.

3.4. Storm flux decomposition

Here, we consider sediment fluxes from a 2.5 day nor'easter during early December 2014 to decompose the sediment flux and determine its most important components. Winds started from the NNW, then quickly evolved to the NNE at an average speed of 8.5 m s^{-1}. Relatively typical for winter nor'easters in Chincoteague Bay, this event was chosen for its well-behaved wind field over the duration of the storm, even though data were not available at 19C and 29B. Note that there was no precipitation during this event.

During the storm, maximum instantaneous fluxes in the channel grew in both flood and ebb directions (Fig. 6). The larger fluxes resulted from increased SSC and also water-level setup near Chincoteague Inlet, enabling larger tidal range and greater tidal flow velocity within the channel (e.g., Fig. 2). On the shoal, where tidal currents were weaker, the instantaneous fluxes were generally in the direction of the wind forcing for the duration of the storm, and the tidal variability was amplified, especially within Sinepuxent Bay. At 20S, which had the strongest tidal velocities of the shoal locations, the instantaneous fluxes were amplified in both flood and ebb directions, similar to the channel locations.

The magnitude and direction of the subtidal sediment flux were different based on geomorphic setting. Shoal subtidal sediment flux was generally aligned with the direction of the wind stress; in the channel, the flux was opposite to the wind. The magnitude of the subtidal flux also increased by a factor of 13–30 during the storm as compared to the calm period immediately preceding the storm.

For this storm, the advective flux was the main component at most sites, and it was in the same direction as the total flux (Fig. 6). The advective flux was generally dominant throughout the study (Table 1). The advective term is interpreted as the "storm flux," the increase in and alteration of SSC caused by subtidal wind events.

Although for this wind event, data were not available at 19C, the dispersive flux was important at the channel sites relatively close to Chincoteague Inlet (19C and 23C) (Table 1). The dispersive flux arises from tidal-timescale correlations between the velocity and SSC. This does not necessarily imply local resuspension, but the importance of the dispersive flux at the southern channel highlights the role of tidal currents at that site, close to Chincoteague Inlet, in resuspending and transporting sediment.

Stokes drift was a small component at most sites (Table 1) and was aligned with the direction of the flood tide. The Stokes flux was greatest close to the inlets, a trend reflective of the larger and more progressive tides at those locations, and southward residual flow at 30B (Section 4.3). Averaged over the full deployment, the vast majority of the flux can be explained by the advective and dispersive components.

3.5. Sediment-flux patterns

Sediment fluxes at the eight stations viewed in the context of wind conditions further illustrate the dynamic geomorphic wind responses in this system. Fig. 7 shows that fluxes are roughly aligned with the bay axis, opposite to the along-bay wind component in the channel, and with the wind at the shoal sites. Fluxes were greatest during the strongest winds, consistent with the results of earlier sections. Within this pattern, additional smaller-scale variability results primarily from local bathymetric features.

In Sinepuxent Bay (30B), fluxes were southwestward for winds to the south and west, indicating that Sinepuxent's channelized nature focuses flow along the channel axis. Only fluxes during winds nearly perpendicular to the bay axis showed evidence of direct wind-driven flow.

At the shoal sites, flux directions were roughly aligned with the wind forcing, subject to influence from bay and local morphology. At 28S, fluxes were aligned NNW–SSE, even under eastward or westward wind forcing. The importance of local channel–shoal bathymetry is evident, as NNW–SSE is the orientation of the local isobaths. Additional local influence in the form of variable fetch drove minimal flux under winds to the west (the direction of least fetch) as compared to stronger flux magnitudes during northward or southward winds. Station 24S is situated on a broad shoal without steep bathymetric gradients nearby, and as a result fluxes were generally well aligned with the wind forcing, although magnitudes tended to be strongest during winds with a significant northward or southward component. At 20S, a winds with a southward component generally resulted in fluxes to the south, and winds with a northward component resulted in fluxes to the NE.

Trends were different along the western side of the bay. In Newport Bay (29B), which is directly connected to the main-bay channel, fluxes were minimal and were opposite to the wind forcing in an along-bay sense. At 27C, winds with a northward component resulted in southward fluxes that were aligned with the local isobaths. Winds with a southward component generally resulted in eastward fluxes; because this is not well aligned with the overall bay orientation it suggests the importance of the local channel–shoal bathymetric contours in modifying the flow and sediment-flux direction. At 23C, fluxes were to the NNW for winds with a southward component, and generally to the SSE

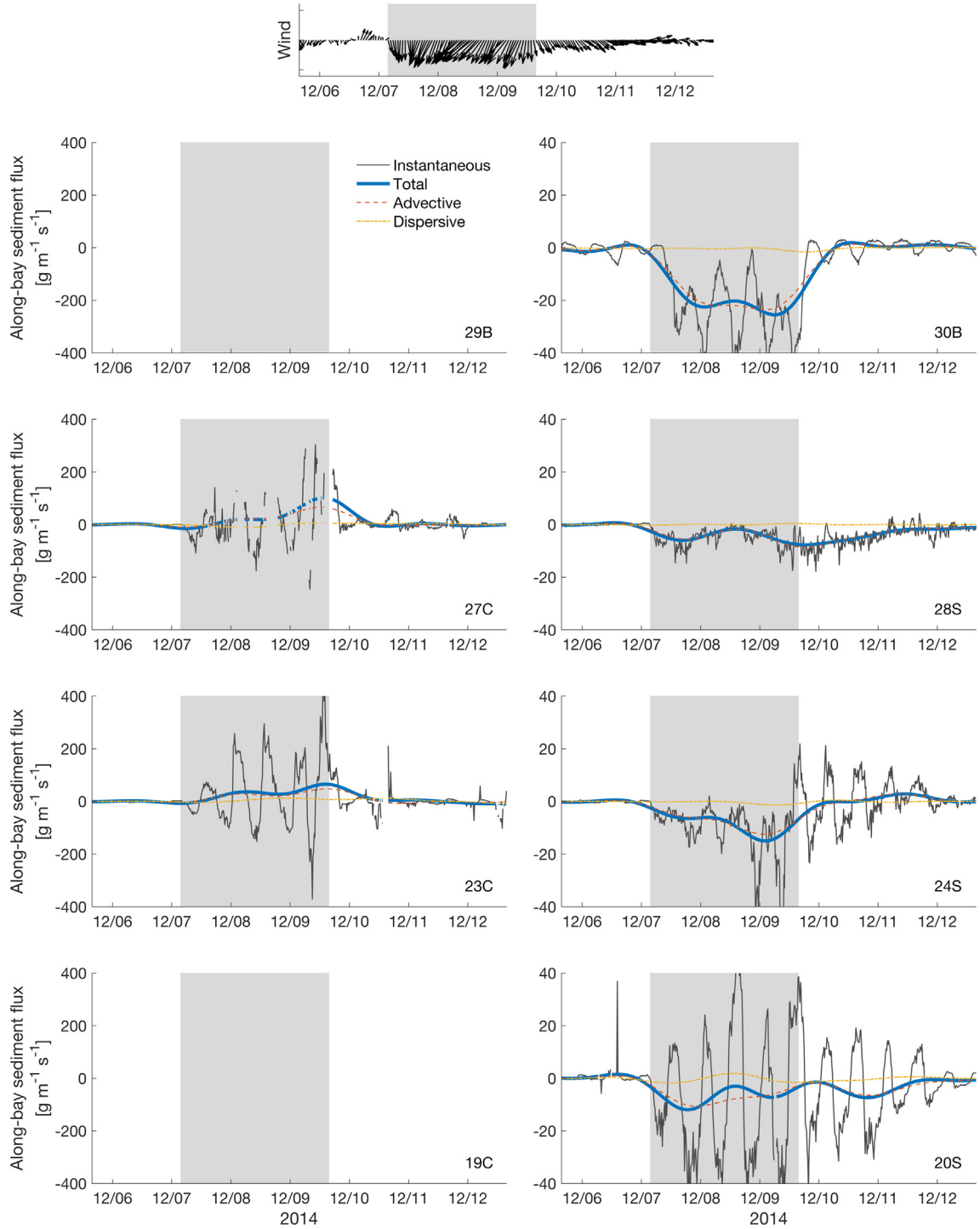

Fig. 6. Instantaneous and decomposed subtidal fluxes at all locations during the southward wind event during December 2014. The subtidal flux is northward at the channel sites and southward at the shoal sites for this southward wind event. The total subtidal flux is almost fully contained in the advective term. No data are available at 19C and 29B during this event because of instrument fouling. Wind is plotted using the velocity convention.

for those with a northward component, directions congruent with the local channel orientation at this site. Wind-influenced trends were less clear at 19C, likely because of the importance of tidal currents at this location in setting the sediment flux.

3.6. Bay-wide sediment budget

The residual sediment flux magnitude and direction at all locations varied with season, particularly within the main bay (Fig. 8).

In Sinepuxent Bay (30B), the net flux for all seasons was southward and ranged from 0.7 to 2.3 g m^{-1} s^{-1}. Flux magnitude to the south during the winter and spring was two to three times greater than during the summer and fall.

In Newport Bay (29B), unit-width flux magnitudes were relatively small (0.4–0.5 g m^{-1} s^{-1}) and directed toward the main bay. The flux magnitudes were comparable to the lower range found at shoal locations within the main bay. The consistent seaward flux direction is congruent with the relatively large freshwater input within Newport

Table 1
Median sediment-flux components (Eq. (1)) expressed as a fraction of the total flux at eight stations for the first deployment. Rows do not sum to one because of the statistic used and because not all components are represented in this table.

Site	Setting	F_{adv}/F	F_{disp}/F	F_{stokes}/F
19C	Channel	0.79	0.64	0.18
20S	Shoal	0.64	0.39	0.18
23C	Channel	0.57	0.61	0.06
24S	Shoal	1.10	0.12	0.02
27C	Channel	0.92	0.24	0.02
28S	Shoal	0.93	0.04	0.01
29B	Newport	0.85	0.28	0.04
30B	Sinepuxent	0.82	0.17	0.09

Bay. That the fluxes were minimal here, closest to the bay's largest fluvial sediment source, is consistent with the small waves in Newport Bay, and also with the assertion of Bartberger (1976) that streams provide little sediment to Chincoteague Bay.

At the northern cross-section (27C/28S), seasonal changes in the characteristics of the sediment dynamics become evident. At 27C, net fluxes during the summer and early fall were to the SE at 1.1 $g\,m^{-1}\,s^{-1}$, to the ENE at 2.9 $g\,m^{-1}\,s^{-1}$ during the late fall and winter, and to the S at 2.25 $g\,m^{-1}\,s^{-1}$ during the late winter and early spring, indicating a dynamic sediment-transport regime that was responsive to seasonal variability. The slight northward component during the October–January deployment was driven primarily by the December 2014 storm event, highlighting the importance of even single events in determining the sediment budget for an entire season at a given location. At 28S, fluxes were to the south during the winter at about 1.3 $g\,m^{-1}\,s^{-1}$; summer fluxes were to the north at 0.20–0.49 $g\,m^{-1}\,s^{-1}$.

Mid bay, at the 23C/24S cross-section, winter fluxes in the channel were northward at 1.8–3.6 $g\,m^{-1}\,s^{-1}$. Summer fluxes were to the southwest at 1.8–1.9 $g\,m^{-1}\,s^{-1}$. Winter fluxes at 24S were to the south at 0.38 $g\,m^{-1}\,s^{-1}$. Taken as a whole, year-integrated fluxes were weakly northward in the channel and southward on the shoal.

Toward the southern end of the bay (19C/20S cross-section), channel fluxes at 19C were generally to the ENE at a rate of 1.8–2.7 $g\,m^{-1}\,s^{-1}$. These rates were balanced by southward rates at 20S of 0.13–1.14 $g\,m^{-1}\,s^{-1}$, with the larger values occurring during the winter deployments.

4. Discussion

4.1. Predicting velocity and sediment-flux patterns

Here we implement a simple wind-driven model that provides insight to the observed subtidal velocities and sediment fluxes. Given the long, narrow nature of the bay and its relatively small inlets, we estimate the wind's influence on flux using a long-lake approximation, following Csanady (1973). The governing equation is

$$c_d \left|\frac{U}{h}\right| \frac{U}{h} = F - gh\frac{d\eta}{dx}, \tag{2}$$

subject to the continuity condition

$$\int_{y_1}^{y_2} U dy = 0, \tag{3}$$

where x and y are the along-bay and cross-bay coordinates, c_d is the drag coefficient, U is the volume transport, U/h is the depth-averaged (but laterally varying) along-bay velocity, F is the density-normalized wind stress, g is gravity, h is the water depth, and η is the water level. The coordinates y_1 and y_2 represent the bay edges.

Assuming minimal flux through the inlets, an along-bay wind stress F is balanced by a pressure gradient $gh\ d\eta/dx$ produced by the wind setup. This pressure gradient produces a return flow which will vary based on topography. Csanady (1973) showed that, where the water is shallower than the mean depth, the wind stress is greater than the pressure gradient and a flow in the direction of the wind develops. Where the water depth is greater than the mean, the pressure gradient exceeds the wind stress and generates a return flow that opposes the wind.

Using the December 2014 storm, we predict the depth-averaged along-bay wind-induced velocity with this model (Fig. 9). The observed along-bay slope $d\eta/dx$, as computed between 19C, 23C, and 27C, was approximately 1×10^{-5}. The mean wind speed, the direction of which was well aligned with the bay, was about 9 $m\,s^{-1}$. We estimate a drag coefficient, following Taylor and Yelland (2001), of 0.0015, resulting in a wind stress $\tau = 0.14$ Pa, with a corresponding density-normalized stress $F = 1.4 \times 10^{-4}\,m^2\,s^{-2}$. Letting $c_d = 2.5 \times 10^{-3}$, we estimate the laterally varying along-bay velocity using Eq. (2), iterating on Eq. (3) to enforce continuity by modifying F, the least constrained measured input. This leads to $F = 1.6 \times 10^{-4}\,m^2\,s^{-2}$, suggesting good agreement of all the input terms.

The modeled lateral velocity profile features upwind flow in the deep regions and downwind flow in the shallow regions; the depth of zero velocity is about 1.6 m (Fig. 9), consistent with observed velocity (Fig. 2b) and sediment-flux (Fig. 7) patterns. Even though the long-lake approximation is not fully appropriate for Chincoteague Bay (particularly the closed-basin assumption), this simple model reproduces the direction and magnitude of the observed currents during this event (Fig. 9). The over-prediction of northward flow within the channel may result from the net southward water flux within the bay, a process which is not accounted for by Csanady (1973). Relaxing the closed-basin assumption by including a southward net flux of 700 $m^3\,s^{-1}$ in Eq. (3) reduces the over-prediction of the channel flow and increases the over-prediction of the shoal flow (Fig. 9b; dotted line).

The predicted volume transport U can be combined with the mean wind–SSC relationship for the channel and shoal sites (Fig. 5) to predict sediment flux for this storm (Fig. 9b; dashed line), which has good agreement with the observed sediment fluxes. The agreement between the observations and the analytical approach reinforces both the consistency and predictability of Chincoteague Bay hydrodynamics and sediment dynamics and that they are strongly influenced by wind forcing.

4.2. Empirical orthogonal function analysis

To investigate forcing mechanisms other than local wind, we use empirical orthogonal functions (EOFs) (Kosambi, 1943; Kundu et al., 1975) to inspect the observed subtidal water levels and flow velocities. EOFs can be used to find spatial and temporal patterns within a data set which can be correlated with potential explanatory variables to provide insight to the important drivers of a system.

Averaged over the eight moorings, the first two orthogonal modes explain the great majority (87% and 11%, respectively) of the total variance of the subtidal water-level time-series. The EOF 1 magnitude is between 0.3 and 0.4 (Fig. 10) at all moorings. There is good correlation ($R^2 = 0.64$) between EOF 1 and low-passed water level at the Ocean City NOAA tide gauge (Fig. 1), suggesting that EOF 1 corresponds to an "offshore" subtidal water level forcing. In this context, 87% of the subtidal water-level variation is forced by the offshore water level, and this influence is approximately equal across the spatial extent of the bay. Correlation coefficients between the time-series constructed with EOF 1 and the measured time-series at each site ranged from 0.70 to 0.99.

There is a good correlation ($R^2 = 0.72$) between EOF 2 and along-bay wind speed, suggesting that EOF 2 is a proxy for the along-bay wind stress. EOF 2 ranges from about − 0.5 at the south end of the bay to about 0.5 in the north, and this pattern is consistent with observed wind setup and set-down (Fig. 2). For northward winds, positive values at the

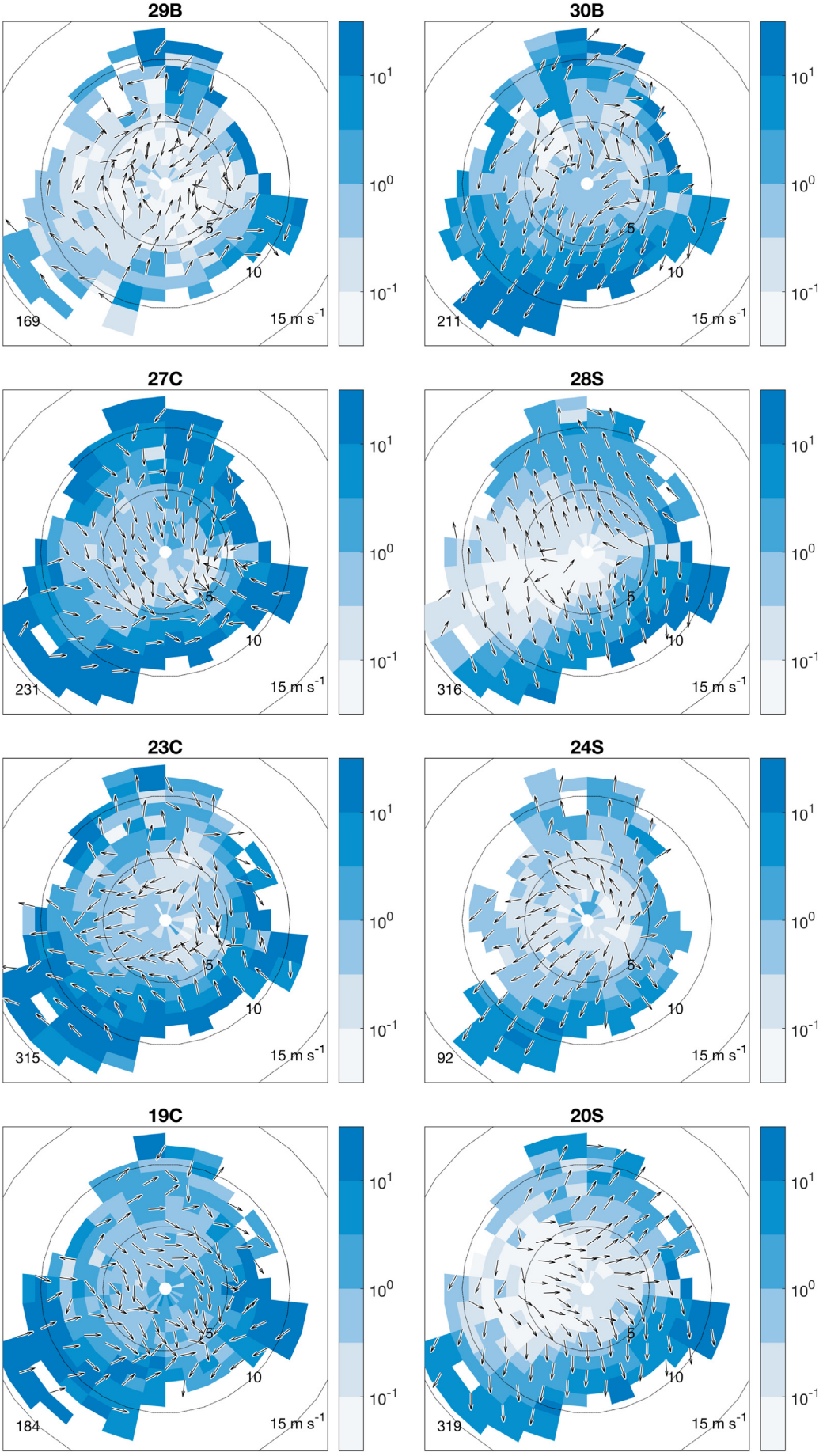

(caption on next page)

Fig. 7. Median unit-width subtidal sediment fluxes in kg m^{-1} as a function of wind speed (distance from center) and direction (angle). Wind is displayed using the velocity convention. Unit-length arrows indicate direction of the sediment flux. Log-scale colors indicate flux magnitudes in each speed–direction bin. Concentric circles indicate 5 m s^{-1} wind speed increments. The total number of aggregated days represented is shown in the lower-left corner of each subplot.

north end of the bay correspond to water-level setup; negative values at the south correspond to water-level setup for southward winds. Comparing a reconstructed time-series using the first and second EOFs to the measured data resulted in R^2 values that ranged from 0.94 to 0.99.

As was the case with water level, the first two EOF modes of the subtidal depth-averaged velocity explain the great majority (91%) of the variance. EOF 1 explains 75% of the variance and is correlated with the along-bay wind forcing ($R^2 = 0.86$), but its magnitude varies among geomorphic setting. At the two southern channel sites (19C and 23C), EOF 1 is ~0.03, indicating the diminished importance of wind where tides are strongest. EOF 1 ranges from 0.1 to 0.7 at the shoal sites and in Sinepuxent Bay. Negative values (about − 0.1) are found at the mid-bay channel site (27C) and Newport Bay. Because the EOF 1 coefficients are positive for the shoal sites and Sinepuxent Bay, a northward wind corresponds to northward velocities at these locations. Conversely, the negative coefficients at the mid-bay channel site and Newport Bay indicates southward flow under northward winds. These results are consistent with those developed in Section 4.1, and also with the patterns in the observed time-series shown in Figs. 2, 7, and 9.

Velocity EOF 2 accounted for an additional 17% of the variance (not shown), but no tested variables were sufficiently correlated with EOF 2 to be considered explanatory. EOF 2 values were positive in Sinepuxent Bay and negative elsewhere, suggesting a mechanism that simultaneously drains and fills the bay via the two inlets: through Chincoteague Inlet for the main bay, and Ocean City inlet for Sinepuxent Bay. This component of the subtidal velocity field has characteristics similar to the tidal-timescale flow routing (Section 3.1). Overall, EOF 2 may be an amalgam of regional atmospheric pressure and water-level variables, of forcing mechanisms that would lead to Ekman flux, or of the propagation of coastally trapped shelf waves (Yankovsky and Garvine, 1998).

The velocity EOFs in Chincoteague are distinct compared to those in other Atlantic back-barrier estuaries. Within Great South Bay, NY and Barnegat Bay, NJ, the majority (70–80%) of the current variance was driven by subtidal coastal sea level leading to simultaneous inflow and outflow through the multiple inlets of those bays (Wong and Wilson, 1984; Chant, 2001). An additional 20% was driven by local winds in those environments. In Chincoteague Bay, these percentages are approximately reversed, with local wind being the most important driver of the subtidal velocity field, and the forcing that leads to simultaneous inflow and outflow through the two inlets being secondary. These patterns are consistent, however, with those found in the Delaware estuary (Wong and Moses-Hall, 1998), just north of Chincoteague Bay.

4.3. Closing the sediment budget

Unit-width sediment budgets at each location (Section 3.6) reinforce the consistency of the opposing water- and sediment-flux directions in the channel and shoal. Here we compare the magnitudes of the observed fine-sediment fluxes to previous estimates of sediment delivery to the bay.

Bartberger (1976) estimated 0.18 Mt y^{-1} of sediment import to Chincoteague Bay, composed of half sand (from the barrier island) and half mud (mainly from shoreline erosion). This estimate, based largely on shoreline-change analyses and bed-sediment distributions, is consistent with more recent, similar studies. For example, Wells et al. (2003) estimated an annual fine-sediment delivery of 0.12 Mt y^{-1} from shoreline erosion in a region north of Public Landing; applying it across the bay results in an estimate of the same order as the mud component computed by Bartberger (1976).

Using the unit-width fluxes measured at 30B to estimate a cross-sectional flux in Sinepuxent Bay under the assumption that velocity and SSC were constant with width results in a southward transport of 0.03–0.11 Mt y^{-1} for this study. The yearly fluxes at 30B alone approach the total sediment delivery estimated from the shoreline change analyses. Although the less-channelized nature of the bay at the other sites makes cross-sectional estimates more challenging, even conservative width estimates produce fluxes of the same order as the

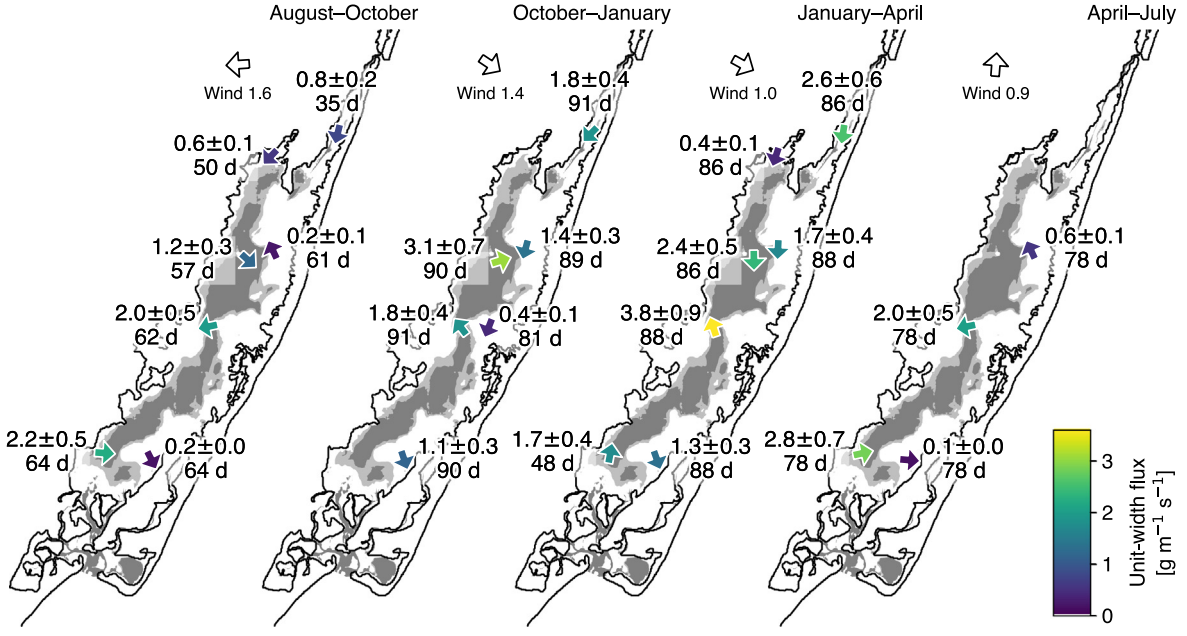

Fig. 8. Average unit-width sediment fluxes by deployment. Arrow colors correspond to magnitude of unit-width flux. Top number indicates flux in g m^{-1} s^{-1}; bottom number indicates number of days represented by average sediment-flux values. Wind arrows indicate mean direction using the velocity convention; numbers below wind arrows show mean wind speed in m s^{-1}.

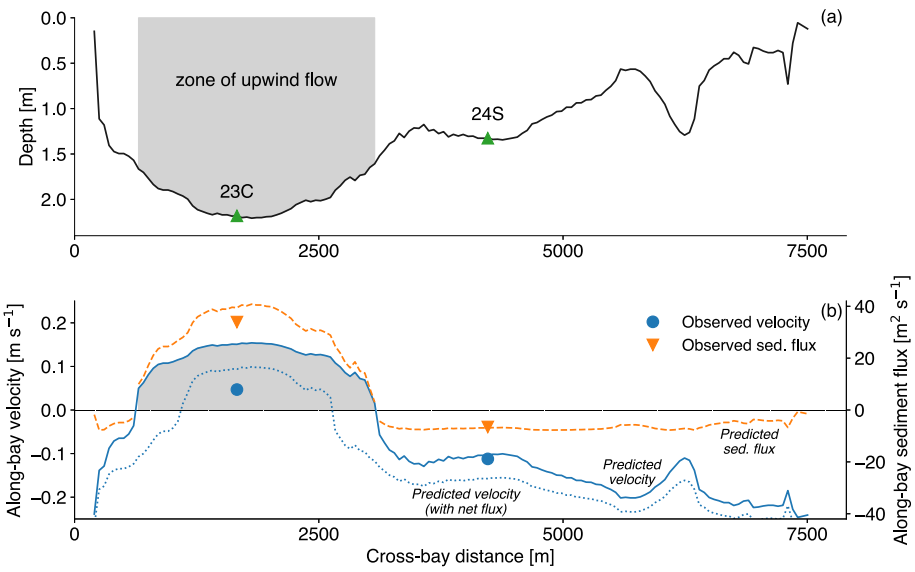

Fig. 9. (a): Bathymetric cross-section of Chincoteague Bay near 23C and 24S. Triangles show approximate station locations and depths. (b): Predicted (lines) and observed (circles) wind-induced velocities, and predicted (lines) and observed (triangles) sediment fluxes at 23C and 24S for the December 2014 wind event. The sign and magnitude of the predicted and observed velocities and sediment fluxes are consistent.

shoreline-change sediment delivery rates. For example, using a representative channel width of 1 km at 23C (about one-third of the actual channel width of ~3.3 km) results in transport rates of 0.04–0.1 Mt y^{-1}. The upper end of this range is the same order as the shoreline-change estimate for delivery to the entirety of the bay. These results suggest that considerably more sediment is transported within the system, temporarily deposited, and subsequently resuspended than is input from external sources. This observation is consistent with previous assertions that back-barrier lagoons internally cycle sediment and receive relatively small amounts of externally sourced sediment that balance material exported from the system (Nichols and Boon, 1994).

The picture becomes different when considering sediment-delivery estimates based on modern (century-scale) geochronology, as well as from borings that integrate Holocene depositional patterns, both of which result in values considerably larger than the shoreline-change figures. Accumulation rates within Chincoteague Bay derived from ^{210}Pb geochronology are in the range 0.17–0.33 cm y^{-1} (Wells et al., 1997, 1998), and 0.51–0.61 g cm^{-2} y^{-1} (Wegner et al., 2011). Considering sediment delivery over the timescale of the Holocene, Bartberger (1976) estimated Holocene sedimentation rates of 0.09–0.18 cm y^{-1}, using borings from Biggs (1970). Assuming bulk densities of 1–2 g cm^{-3}, the ^{210}Pb values correspond to yearly sediment-delivery rates 0.6–2.5 Mt y^{-1}, and the Holocene values to 0.3–1.4 Mt y^{-1}, considerably larger masses (up to an order of magnitude greater) than the fine-grained estimates from shoreline-change

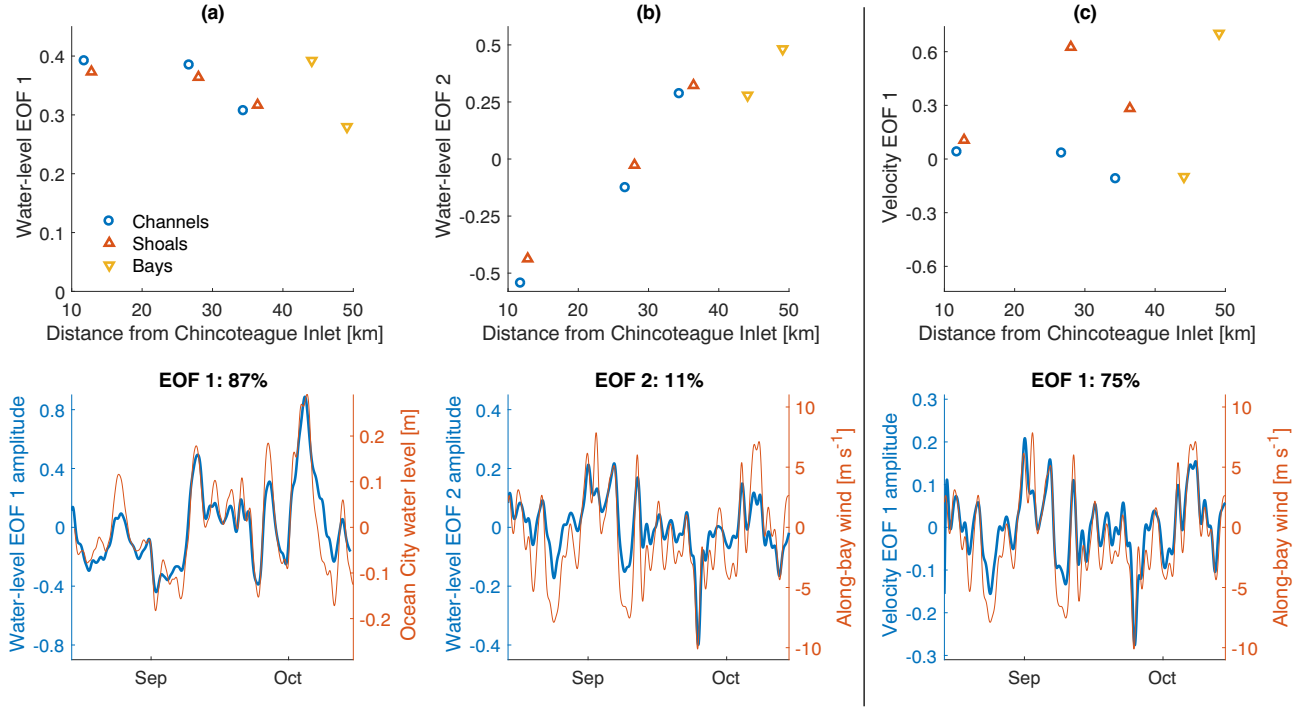

Fig. 10. EOF analysis of low-passed water level and along-bay velocity. (a) and (b): Water-level EOFs. EOF 1 is interpreted as the "offshore" water level, and EOF 2 is interpreted as local setup from wind forcing. Here, negative along-bay winds are those with a southward component. (c): Along-bay velocity EOF. EOF 1 is strongly associated with the along-bay wind forcing.

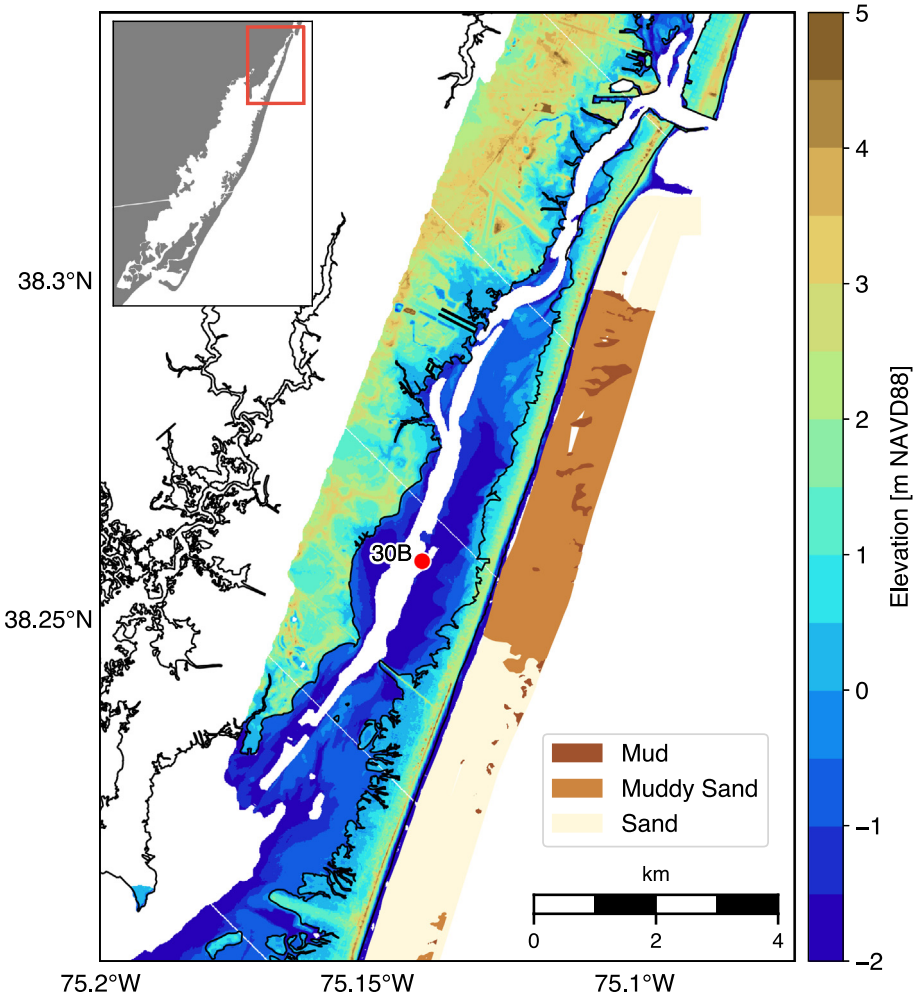

Fig. 11. NOAA topo-bathy LiDAR collected during 2014 in the Sinepuxent Bay area (National Oceanic and Atmospheric Administration, 2015) and nearshore sediment characteristics (Wells et al., 2014). Note low-elevation barrier dune crest elevations and zone of muddy sand north of 30B.

analyses.

Bartberger (1976) attributed the discrepancy between the shoreline-change and Holocene estimates to anomalously low modern sediment delivery following the recent (last 200 years) closing of multiple inlets to Chincoteague Bay. This hypothesis is not borne out, however, by the ^{210}Pb geochronology, which is applicable over approximately the past century. Indeed, the relative consistency of the ^{210}Pb and Holocene estimates could suggest that the shoreline change analyses are missing an important additional sediment source.

From where might additional sediment be sourced? One possibility is delivery of sediment through the two present inlets. This southward flux through Sinepuxent Bay suggests delivery of sediment from a northern source, perhaps via Ocean City Inlet. Another possibility is that some of the fine sediment comes from a relatively fine-grained sediment source in the Assateague Island nearshore (Fig. 11). The low elevation of the barrier dune in this region enables frequent washovers, as well as the creation of temporary barrier breaches and storm-surge channels (e.g., the opening of breaches in the area just north of 30B during a 1962 storm; Seminack and McBride, 2015). These features could facilitate import of this fine-grained material, which may then be temporarily stored and fluxed southward past 30B and delivered to the main bay.

4.4. Influence of geomorphology on sediment-transport processes

Although the bathymetric variability in Chincoteague Bay is subtle, of order 1–2 m, this variability has dramatic importance in the response of the bay to external inputs (e.g., tides and winds). In the channel, tidal currents are relatively strong and are the dominant feature of the instantaneous velocity. When wind increases, tidal range and tidal currents become larger (Fig. 2), and although the wind induces a subtidal return flow, the flow is not immediately obvious when inspecting the velocity time-series. In contrast, wind is most important on the shoals, sometimes to the extent that there are no discernible tidal currents during windy periods (Fig. 2).

The SSC response is also highly dependent on site geomorphology. Even though the bed stress is not significantly greater at the channel sites than the shoals (Fig. 4), the resultant SSC is much greater because of the more-erodible sediment present there. In contrast, the coarser sediment on the shoals has a higher critical shear stress, and after resuspension, weaker shoal currents do not move the suspended material as far as they do in the channel.

These tidal- and seasonal-scale observations take on additional meaning when viewed in the context of longer-term morphological evolution. Chincoteague Bay hydrodynamics exist in congruence with regional flux patterns, and the bay facilitates the southward movement of regional water masses (and likely sediment). The overall trajectory of Assateague Island is that of southward drift: Toms Cove Hook, the southernmost point of Assateague Island, migrated southward at an average rate of about 20 m y^{-1} during the 20th century (National Park Service, 2011). The net nearshore sediment-transport direction is also to the southwest in this region (Belknap and Kraft, 1985; Schupp, 2013;

Fenster et al., 2016).

Within the bay, overwash which occurs during storms is reshaped by this southward flow; shoals within Chincoteague migrate southward during stormy, winter periods (Ganju et al., 2016). Finer-grained sediment in the channel is transported northward during these same periods, implying a larger-scale sedimentary circulation pattern within the bay, with fluxes in opposing directions in the channel and shoal (Section 4.1). These contrasting patterns highlight the importance of viewing back-barrier environments as coupled systems (Walters et al., 2014; Miselis et al., 2016). As a relatively undeveloped barrier-island system, natural overwash and migration are allowed to occur in Chincoteague Bay, in contrast to other, more altered East-coast back-barrier systems, where sediment may be trapped in dredged area or urbanized settings. In those altered environments, the coupled parts of the system are unable to evolve in concert with each other (Miselis and Lorenzo-Trueba, 2017).

5. Conclusion

The overall patterns of water and sediment fluxes within Chincoteague Bay are controlled by wind forcing and tides, and dynamics within the bay exist in concert with larger-scale regional flux patterns. Storms have a disproportionate influence on the net sediment flux, and future variability of storm patterns could have ramifications on the geomorphic trajectory of the system. Despite being a shallow environment with subtle bathymetric features, distinct trends were observed in each geomorphic setting (channel, shoal, bay), which also varied with season. The magnitude of the observed sediment fluxes was in general greater than previous estimates of sediment delivery to Chincoteague Bay, suggesting either intense internal recycling of sediment or the possibility of an additional external sediment source not accounted for in previous studies. The observed sediment-transport patterns help inform studies of future geomorphic change of back-barrier estuaries over seasonal and longer timescales, and establish a conceptual model of back-barrier sediment transport in an undeveloped estuary.

Acknowledgments

This study was part of the Estuarine Physical Response to Storms project (GS2-2D), supported by the Department of the Interior Hurricane Sandy Recovery program. This paper benefited from conversations with Alfredo Aretxabaleta and the comments of Jenna Brown and three anonymous reviewers. Brian Andrews generated the Chincoteague bathymetric grid. Data analyzed in this study may be obtained from the USGS Oceanographic Time-Series Database at https://doi.org/10.5066/F7DF6PBV. Any use of trade, firm, or product names is for descriptive purposes only and does not imply endorsement by the U.S. Government.

References

Aretxabaleta, A.L., Butman, B., Ganju, N.K., 2014. Water level response in back-barrier bays unchanged following Hurricane Sandy. Geophys. Res. Lett. 41, 3163–3171. https://doi.org/10.1002/2014GL059957.

Bartberger, C.E., 1976. Sediment sources and sedimentation rates, Chincoteague Bay, Maryland and Virginia. J. Sediment. Petrol. 46, 326–336. https://doi.org/10.1306/212F6F50-2B24-11D7-8648000102C1865D.

Belknap, D.F., Kraft, J.C., 1985. Influence of antecedent geology on stratigraphic preservation potential and evolution of Delaware's barrier systems. Mar. Geol. 63, 235–262. https://doi.org/10.1016/0025-3227(85)90085-4.

Biggs, R.B., 1970. The Origin and Geological History of Assateague Island, Maryland and Virginia. Technical Report. Natural Resources Institute, University of Maryland.

Carruthers, T., Beckert, K., Dennison, B., Thomas, J., Saxby, T., Williams, M., Fisher, T., Kumer, J., Schupp, C., Sturgis, B., Zimmerman, C., 2011. Assateague Island National Seashore Natural Resource Condition Assessment. Technical Report. Natural Resource Report NPS/ASIS/NRR–2011/405.

Casey, J., Wesche, A., 1981. Marine Benthic Survey of Maryland's Coastal Bays: Part I, Spring and Summer Periods, 1981. Technical Report. Maryland Department of Natural Resources, Annapolis, Maryland.

Chant, R.J., 2001. Tidal and subtidal motion in a shallow bar-built multiple inlet/bay system. J. Coast. Res. SI32, 102–114.

Csanady, G., 1973. Wind-induced barotropic motions in long lakes. J. Phys. Oceanogr. 3, 429–438.

Defne, Z., Ganju, N.K., 2015. Quantifying the residence time and flushing characteristics of a shallow, back-barrier estuary: application of hydrodynamic and particle tracking models. Estuar. Coasts 38, 1719–1734. https://doi.org/10.1007/s12237-014-9885-3.

Dronkers, J., 1986, Aug, Aug. Tidal asymmetry and estuarine morphology. Neth. J. Sea Res. 20, 117–131. https://doi.org/10.1016/0077-7579(86)90036-0.

Dyer, K., 1974, Jul, Jul. The salt balance in stratified estuaries. Estuar. Coast. Mar. Sci. 2, 273–281. https://doi.org/10.1016/0302-3524(74)90017-6.

Ellis, A.M., Marot, M.E., Wheaton, C.J., Bernier, J.C., Smith, C.G., 2015. A Seasonal Comparison of Surface Sediment Characteristics in Chincoteague Bay, Maryland and Virginia, USA. Technical Report. U.S. Geological Survey Open-File Report 2015-1219https://doi.org/10.3133/ofr20151219.

Fenster, M.S., Dolan, R., Smith, J.J., 2016. Grain-size distributions and coastal morphodynamics along the southern Maryland and Virginia barrier islands. Sedimentology 63, 809–823. https://doi.org/10.1111/sed.12239.

Ganju, N.K., Suttles, S.E., Beudin, A., Nowacki, D.J., Miselis, J.L., Andrews, B.D., 2016. Quantification of storm-induced bathymetric change in a back-barrier estuary. Estuar. Coasts. https://doi.org/10.1007/s12237-016-0138-5.

Goodrich, D.M., 1988. On meteorologically induced flushing in three U.S. East Coast estuaries. Estuar. Coast. Shelf Sci. 26, 111–121. https://doi.org/10.1016/0272-7714(88)90045-5.

Johnson, D., 2011. DIWASP, A Directional Wave Spectra Toolbox for MATLAB®: User Manual. Technical Report. Centre for Water Research, University of Western Australia.

Kang, X., Xia, M., Pitula, J.S., Chigbu, P., 2017. Dynamics of water and salt exchange at Maryland Coastal Bays. Estuar. Coast. Shelf Sci. https://doi.org/10.1016/j.ecss.2017.03.002.

Kjerfve, B., 1994. Coastal Lagoons. In: Kjerfve, B. (Ed.), Coastal Lagoon Processes. Elsevier, pp. 1–8.

Kosambi, D.D., 1943. Statistics in function space. J. Indian Math. Soc. 7, 76–88.

Krantz, D.E., Schupp, C.A., Spaur, C.C., Thomas, J.E., Wells, D.V., 2009. Dynamic systems at the land-sea interface. In: Shifting Sands: Environmental and Cultural Change in Maryland's Coastal Bays. IAN Press, Cambridge, MD, pp. 193–230.

Kundu, P.K., Allen, J., Smith, R.L., 1975. Modal Decomposition of the Velocity Field near the Oregon Coast. https://doi.org/10.1175/1520-0485(1975)005<0683:MDOTVF>2.0.CO;2.

Leonardi, N., Ganju, N.K., Fagherazzi, S., 2016. A linear relationship between wave power and erosion determines salt-marsh resilience to violent storms and hurricanes. Proc. Natl. Acad. Sci. U. S. A. 113, 64–68. http://www.pnas.org/lookup/doi/10.1073/pnas.1510095112https://doi.org/10.1073/pnas.1510095112.

Madsen, O.S., 1994. Spectral wave-current bottom boundary layer flows. Coastal Engineering Proceedings 1, 384–398. https://doi.org/10.9753/icce.v24.

Miselis, J.L., Andrews, B.D., Nicholson, R.S., Defne, Z., Ganju, N.K., Navoy, A., 2016. Evolution of mid-Atlantic coastal and back-barrier estuary environments in response to a hurricane: implications for barrier-estuary connectivity. Estuar. Coasts 39, 916–934. https://doi.org/10.1007/s12237-015-0057-x.

Miselis, J.L., Lorenzo-Trueba, J., 2017. Natural and human-induced variability in barrier-island response to sea level rise. Geophys. Res. Lett. 44https://doi.org/10.1002/2017GL074811. 11,922–11,931.

National Oceanic and Atmospheric Administration, 2015. 2014 NOAA Post Hurricane Sandy Topobathymetric LiDAR Mapping for Shoreline Mapping. https://coast.noaa.gov/dataviewer/#/lidar/search/where:ID=4800.

National Park Service, 2011. Toms Cove Shoreline Change. https://www.nps.gov/asis/learn/nature/upload/Tom-s-Cove-Change44.pdf.

National Park Service, 2017. NPS Inventory and Monitoring Program. https://science.nature.nps.gov/im/.

Nichols, M., Allen, G., 1981. Sedimentary processes in coastal lagoons. In: Coastal lagoon research, present and future. Proceedings of an Unesco/IABO Seminar: Unesco Technical Papers in Marine Science 33, pp. 27–79.

Nichols, M.M., Boon, J.D., 1994. Sediment transport processes in coastal lagoons. In: Kjerfve, B. (Ed.), Coastal Lagoon Processes. Elsevier Science B.V., pp. 157–219.

Oertel, G.F., 1985. The barrier island system. Mar. Geol. 63, 1–18. https://doi.org/10.1016/0025-3227(85)90077-5.

Postma, H., 1967. Sediment Transport and Sedimentation in the Estuarine Environment. In: Lauff, G.H. (Ed.), Estuaries. American Association for the Advancement of Science, pp. 158–179.

Ralston, D.K., Geyer, W.R., Lerczak, J.A., Scully, M., 2010. Structure, variability, and salt flux in a strongly forced salt wedge estuary. J. Geophys. Res. Oceans 115 (C6), 1–21. https://doi.org/10.1029/2009JC006061.

Ralston, D.K., Geyer, W.R., Warner, J.C., 2012, oct, oct. Bathymetric controls on sediment transport in the Hudson River estuary: lateral asymmetry and frontal trapping. J. Geophys. Res. 117, C10013. https://doi.org/10.1029/2012JC008124.

Schupp, C., 2013. Assateague Island National Seashore Geologic Resources Inventory Report. Technical Report. Natural Resource Report NPS/NRSS/GRD/NRR–2013/708, Fort Collins, Colorado.

Seminack, C.T., McBride, R.A., 2015. Geomorphic history and diagnostic features of former tidal inlets along Assateague Island, Maryland-Virginia: a life-cycle model for inlets along wave-dominated barrier islands. Shore & Beach 83 (3), 3–24.

Soulsby, R., 1997. Dynamics of marine sands. Telford, London, pp. 272.

van Straaten, L., Kuenen, P.H., 1958. Tidal action as a cause of clay accumulation. J. Sediment. Petrol. 28, 406–413.

Stutz, M.L., Pilkey, O.H., 2011. Open-ocean barrier islands: global influence of climatic, oceanographic, and depositional settings. J. Coast. Res. 27, 207–222. https://doi.org/

10.2112/09-1190.1.
Suttles, S.E., Ganju, N.K., Brosnahan, S.M., Montgomery, E.T., Dickhudt, P.J., Beudin, A., Nowacki, D.J., Martini, M.A., 2017. Summary of Oceanographic and Water-quality Measurements in Chincoteague Bay, Maryland and Virginia, 2014–15. Technical Report. U.S. Geological Survey Open-File Report 2017-1032.
Taylor, P.K., Yelland, M.J., 2001. The dependence of sea surface roughness on the height and steepness of the waves. J. Phys. Oceanogr. 31 (1996), 572–590. https://doi.org/10.1175/1520-0485(2001)031<0572:TDOSSR>2.0.CO;2.
Walters, D., Moore, L.J., Vinent, O.D., Fagherazzi, S., Mariotti, G., 2014. Interactions between barrier islands and backbarrier marshes affect island system response to sea level rise: insights from a coupled model. J. Geophys. Res. Earth Surf. 119, 2013–2031. https://doi.org/10.1002/2014JF003091.
Wegner, C., Andreucci, S., Odhiambo, B.K., 2011. Sedimentation rates and trace metal input history in Chincoteague lagoon-marsh system derived from Pb-210 and Cs-137 chronology. In: Geological Society of America Southeastern Section - 60th Annual Meeting.
Wells, D., Harris, S., Hill, J., Park, J., Williams, C., 1997. The Shallow Sediments of the Upper Chincoteague Bay area in Maryland: Physical and Chemical Characteristics. Technical Report. Maryland Geological Survey File Report 97-2.
Wells, D.V., Conkwright, R.D., Ortt Jr., R.A., Van Ryswick, S., Younger, R., 2014. Inventory of Physical and Benthic Habitats and Ocean Resources within the Nearshore Boundary of Assateague Island National Seashore: Part I-Geophysical Framework. Technical Report. Natural Resource Technical Report NPS/XXXX/NRTR–20XX/XXX. National Park Service, Fort Collins, Colorado.
Wells, D.V., Hennessee, E.L., Hill, J.M., 2003. Shoreline Erosion as a Source of Sediments and Nutrients: Middle Coastal Bays, Maryland. Technical Report. Maryland Geological Survey. http://www.mgs.md.gov/coastal/pub/mcbfinal.pdf.
Wells, D.V., Hill, J.M., Park, M.J., Williams, C.P., 1998. The Shallow Sediments of the Middle Chincoteague Bay area in Maryland: Physical and Chemical Characteristics. Technical Report. Maryland Geological Survey File Report 98-1.
Wells, J.T., Kim, S.-Y., 1989. Sedimentation in the Albemarle-Pamlico lagoonal system: synthesis and hypotheses. Mar. Geol. 88, 263–284. https://doi.org/10.1016/0025-3227(89)90101-1.
Wong, K.-C., Moses-Hall, J.E., 1998. On the relative importance of the remote and local wind effects to the subtidal variability in a coastal plain estuary. J. Geophys. Res. 103, 18393–18404.
Wong, K.-C., Wilson, R.E., 1984. Observations of low-frequency variability in Great South Bay and relations to atmospheric forcing. J. Phys. Oceanogr. 14, 1893–1900. https://doi.org/10.1175/1520-0485(1984)014<1893:OOLFVI>2.0.CO;2.
Xie, L., Eggleston, D., 1999. Computer simulations of wind-induced estuarine circulation patterns and estuary-shelf exchange processes: the potential role of wind forcing on larval transport. Estuar. Coast. Shelf Sci. 49, 221–234.
Yankovsky, A.E., Garvine, R.W., 1998. Subinertial dynamics on the inner New Jersey shelf during the upwelling season. J. Phys. Oceanogr. 28, 2444–2458. https://doi.org/10.1175/1520-0485(1998)028<2444:SDOTIN>2.0.CO;2.